Structural insights into the AapA1 toxin of Helicobacter pylori

Dursun Nizam Korkut, Isabel D. Alves, Alexander Vogel, Sandrine Chabas, Cynthia M. Sharma, Denis Martinez, Antoine Loquet, Gilmar Salgado, Fabien Darfeuille

Structural insights into the AapA1 toxin of *Helicobacter pylori*

Dursun Nizam Korkut[1,2,#], Isabel D. Alves[3], Alexander Vogel[4], Sandrine Chabas[1], Cynthia M. Sharma[5], Denis Martinez[3], Antoine Loquet[3], Gilmar F. Salgado[1,2,*] and Fabien Darfeuille[1,*]

[1] INSERM, U1212, CNRS UMR 5320, Univ. Bordeaux, Laboratoire ARNA, F-33076 Bordeaux, France
[2] Univ. Bordeaux, IECB, Laboratoire ARNA, F-33600 Pessac, France
[3] Univ. Bordeaux, CBMN-UMR 5248 CNRS, IPB, F-33600 Pessac, France
[4] Univ. Leipzig, Institute for Medical Physics and Biophysics, G-04107 Leipzig, Germany
[5] University of Würzburg, Institute of Molecular Infection Biology, Josef-Schneider-Str. 2, D-97080, Würzburg, Germany

* To whom correspondence should be addressed. INSERM, U1212, Laboratoire ARNA, F-33076 Bordeaux, France
Email: fabien.darfeuille@inserm.fr, gilmar.salgado@u-bordeaux.fr; Tel : +33557574565

ARTICLE INFO

Keywords: bacterial toxin, toxin-antitoxin, *Helicobacter pylori*, transmembrane domain, small membrane protein

ABSTRACT

Background: We previously reported the identification of the aapA1/IsoA1 locus as part of a new family of toxin-antitoxin (TA) systems in the human pathogen *Helicobacter pylori*. AapA1 belongs to type I TA bacterial toxins, and both its mechanism of action towards the membrane and toxicity features are still unclear.

Methods: The biochemical characterization of the AapA1 toxic peptide was carried out using plasmid-borne expression and mutational approaches to follow its toxicity and localization. Biophysical properties of the AapA1 interaction with lipid membranes were studied by solution and solid-state NMR spectroscopy, plasmon waveguide resonance (PWR) and molecular modeling.

Results: We show that despite a low hydrophobic index, this toxin has a nanomolar affinity to the prokaryotic membrane. NMR spectroscopy reveals that the AapA1 toxin is structurally organized into three distinct domains: a positively charged disordered N-terminal domain (D), a single α-helix (H), and a basic C-terminal domain (R). The R domain interacts and destabilizes the membrane, while the H domain adopts a transmembrane conformation. These results were confirmed by alanine scanning of the minimal sequence required for toxicity.

Conclusion: Our results have shown that specific amino acid residues along the H domain, as well as the R domain, are essential for the toxicity of the AapA1 toxin.

General Significance: Untangling and understanding the mechanism of action of small membrane-targeting toxins are difficult, but nevertheless contributes to a promising search and development of new antimicrobial drugs.

HIGHLIGHTS

The AapA1 toxin of the human pathogen *Helicobacter pylori* is a small membrane protein

AapA1 specifically targets the inner membrane of this bacterium

AapA1 adopts an alpha-helical structure (H) flanked by two positively charged domains (D and R)

Specific amino acid residues along the helix together with the C-ter are essential for the toxicity of this small protein

---

1 INTRODUCTION

Toxin-antitoxin (TA) systems are simple genetic modules composed of two genes: one gene encodes a toxin, and the second an antitoxin that counteracts the activity of the toxin or its expression. The toxin gene product induces bacterial growth arrest or death of the bacterium by inhibiting essential cellular processes such as replication, protein synthesis or cell division [1]. The functions of these TA systems have been linked either directly or indirectly to virulence and antibiotic persistence in many bacterial pathogens [2, 3]. TA systems are classified into six types depending on the nature and mode of action of the antitoxin [1]. In type I TA system, the antitoxin is an antisense RNA that inhibits toxin synthesis, by inhibiting its translation or activating its mRNA degradation, or by both mechanisms [4-6]. With the exceptions of two TA systems, (SymE/SymR) and (RalA/RalR), toxins belonging to type I TA systems are generally small hydrophobic proteins of less than 60 aa that contain a potential alpha-helical transmembrane (TM) domain [4, 5, 7]. However, experimental validation of the TM segment has only been performed for a few toxins, such as TisB and Ibs in *Escherichia coli* [8-10], Fst in *Enterococcus faecalis* [11], and SprA1 in *Staphylococcus aureus* [12].

Despite this common feature, type I toxins display different modes of action. Previous studies have typically relied on experiments of ectopic overexpression of the toxin. Due to the hydrophobic nature of the peptide and their similarity to phage holins [13] or cationic antimicrobial peptides [14], they exert their toxic activity by altering membrane integrity [15]. Indeed, membrane depolarization or permeabilization, followed by a decrease of intracellular ATP, is a common mechanism for many type I toxins such as Hok [16, 17], DinQ [18], Fst [19] Ibs [9] and TisB [20]. As a possible exception to this paradigm, overexpression of BsrG peptide in *Bacillus subtilis* does not induce toxicity by disrupting membrane potential nor affecting cellular ATP-levels. Instead, BsrG produces membrane invaginations that cause delocalization of the cell wall synthesis machinery followed by autolysis [21]. Other exceptions may include the detergent effect and membrane thinning well known for antimicrobial peptides [8]. It is also not excluded that some of these transmembrane peptides may

exert their toxic action by interacting with membrane protein partners such as the SidA and MgtS peptides [22, 23].

Despite the fact that most type I toxins are small membrane peptides, they display a strong diversity in length and amino acid sequence [15]. Sequence requirements for toxicity have been determined by saturated mutagenesis approaches for the Ibs and Fst toxins [9, 24], which revealed that only a few residues are critical for toxicity and clustered in small but functional domains. However, a lack of sequence conservation between these small membrane peptides hinders prediction of type I TA systems by homology searches [25]. Indeed, type I TA systems have so far only been described in Proteobacteria and Firmicutes [4], in contrast to the more widely distributed type II and type III TA systems [26]. We have recently characterized a new TA system in the human gastric pathogen *Helicobacter pylori* [27]. This *aapA1*/IsoA1 module was initially discovered by global transcriptome analysis in the *H. pylori 26695* strain among five other putative type I TA system [28]. It belongs to a new family of TA systems that is well conserved in the genomes of diverse *Helicobacter* and *Campylobacter* strains. The *aapA1* gene of this tightly regulated genetic module codes for a small peptide of 30 amino acids whose expression is strongly toxic in *H. pylori* [27].

In this work, we investigate the biophysical and structural properties of the AapA1 toxin that enable membrane targeting and toxicity following its expression in *H. pylori*. We used a combination of *in vitro* biophysical techniques such as liquid- and solid-state nuclear magnetic resonance (NMR), Plasmon Waveguide Resonance (PWR) and Molecular Dynamics (MD), complemented with cellular experiments to better understand the molecular determinants of AapA1 toxicity. We report the existence of a minimal sequence requirement for toxicity, and particularly the importance of two highly conserved positively charged amino acids (KR) at its C-terminus. The interaction of the toxin with the membrane was confirmed *in vivo* and thoroughly followed by PWR, solid-state NMR and MD simulations. These experiments revealed the structure of the peptide, affinity to the membrane in the nanomolar range, and a noticeable perturbation of the membrane organization. The AapA1 toxin folds into three functional domains, as observed by NMR, with a putative transmembrane α-helical segment, flanked by two positively charged domains that appear to be unfolded. Strikingly the first 8 amino acid residues are not required for toxicity, in contrast to the two positively charged residues at the C-terminus.

---

2 MATERIAL AND METHODS

2.1 E. coli strains and media culture conditions.

All bacterial strains and plasmids used in this work are listed in Supplementary Table S1 and S2, respectively. *Escherichia coli* C43 (DE3) pLysS (55) was used to monitor the toxicity of AapA1 in truncation and alanine scanning experiments. *E. coli* strains were grown at 37°C in lysogeny broth (LB) with shaking at 180 rpm. Antibiotics were added when necessary at the following concentrations: 100 µg/mL ampicillin, 30 µg/ml chloramphenicol, 25 µg/mL kanamycin. For overexpression

experiments in *E. coli* strains, either isopropyl β-D-1-thiogalactopyranoside (IPTG) or L-(+)-arabinose were used at a final concentration of 0.25 mM and 13.3 mM, respectively.

2.2 Cloning experiments for AapA1 expression in E. coli strains.

For AapA1 expression experiments in the C43 *pLysS* strain, the AapA1 coding sequence or its truncated form were amplified by single-step PCR from genomic DNA (*H. pylori* 26695 strain) (see Supplementary Table S3 for primer list) and ligated into the NdeI and BamHI sites of the pET-MCN plasmid (Supplementary Table S2). PCR was performed with Phusion High- Fidelity DNA polymerase (ThermoFischer). PCR products and plasmids were digested with NdeI and BamHI restrictions enzymes (Promega). Ligation was done using T4 DNA ligase (Promega). Alanine scanning was carried out by site directed mutagenesis, using end-mutagenic and overlapping oligonucleotides listed in Supplementary Table S3. DH5a chemically competent cells (ThermoFischer Scientific) were transformed with the ligation mixtures according to the manufacturer's instructions. Plasmid DNA was purified by the Sigma-Aldrich kit according to the manufacturer's instructions. Inserts were sequenced at Eurofins Laboratories (Germany). Plasmids were then transformed into homemade *E. coli* BL21 (DE3) pLysS chemically competent cells.

2.3 Cloning experiments for AapA1 toxin expression in H. pylori strains.

Shuttle vectors (pILL2157bis) expressing the AapA1 peptide alone (pAapA1), or fused to the sequential affinity peptide tag (pAapA1-SPA) under an IPTG- inducible promoter, were cloned as previously described (26). In both cases the nucleotide sequence of the AapA1 contained the two synonymous mutations inactivating the IsoA1 antitoxin promoter (**Fig. 1A**). The AapA1 DNA sequence was amplified with the FD212/FD680 primer pair from the pA1 plasmid (26). The AapA1-SPA DNA sequence was amplified with the FD213/FD591 primers from the pCSN58-2 plasmid. Both plasmids were then introduced by conjugation into the B128 *H. pylori* strain deleted for the endogenous *aapA1*/IsoA1 locus (H17 strain, see supplementary Table S1) as previously described (26).

2.4 H. pylori growth and cell fractionation.

Frozen stocks of *H. pylori* H131 (pAapA1) and H135 (pAapA1-SPA) strains were recovered by 48 h growth on Columbia agar plates supplemented with 7% laked horse blood, the Dent antibiotic cocktail (Oxoid, Baingstoke, UK) and 8 µg/ml of chloramphenicol. Liquid cultures were carried out in Brain-Heart Infusion medium (BHI) (Oxoid, Baingstoke, UK) supplemented with 10% decomplemented Fetal Calf Serum (FCS, Eurobio) and chloramphenicol (8 µg/ml). Both solid and liquid cultures were incubated at 37°C under microaerobic conditions (6%O_2, 10% CO_2, 84% N_2) using an Anoxomat atmosphere generator (MART Microbiology). For analysis of growth cultures, bacteria harvested from plates were inoculated at an OD_{600} of 0.5 into tubes containing 5 mL BHI liquid medium as described above, with shaking at 180 rpm. After 8 h, these pre-cultures were diluted to an OD_{600} of 0.02 into flasks containing 30 mL media, shaking at 110 rpm and incubated at 37°C under microaerobic conditions. IPTG at 1 mM final concentation was added after 16 hours of culture. Cells were

harvested 7 hours after induction by 10 min centrifugation at 6000 *g* and 4°C, washed twice in phosphate-buffered saline medium (PBS) prior to their disruption in 5 mL of buffer B (10 mM Tris-HCl pH 8, containing 1 mM DTT and 1 mM PMSF) by sonication for 30 s at 3 watts using a Sonifier 150 (Branson). Cell debris were removed by centrifugation at 3000 *g* for 20 min at 4°C, and supernatants containing cytoplasm and membrane fractions were collected as total extracts. A sample of total extracts (800 µL) was frozen and the remaining supernatant (4.2 mL) was subjected to ultracentrifugation (125 000 x g, 2 hours, 4°C). Samples from the supernatant containing the cytoplasm were collected and frozen while pellets containing total membranes were resuspended in 1/5 of the initial volume (840 µL) in buffer B. For separation of inner and outer membrane, 100 µL of total membranes were collected by ultracentrifugation for 1 h at 125000 *g* and resuspended in buffer B supplemented with 1% N-lauroyl sarcosine (m/v, Sigma), incubated for 1 h at 4 °C prior to ultracentrifugation (125 000 x g, 2 hours, 4°C). Samples of inner membrane fractions from supernatants were frozen. Pellets were washed twice with 15 mL of buffer B and concentrated on Amicon Ultra-15 3K (Millipore). In each fraction, protein amounts were calibrated using the Bradford DC Protein Assay (Biorad) with bovine serum albumin (BSA) as a standard.

2.5 Immunoblot assays.

A fraction equivalent to the cells in OD_{600} = 0.1 was loaded and separated onto a 10% Tris Tricine gel (resolving: 10% acrylamide/bisacrylamide 29:1, 1M Tris pH 8.45, SDS 0.1%, glycerol 10%; stacking: 4% acrylamide/bisacrylamide 29:1, 1M Tris pH 8.45, SDS 0.1%,). Gels were run at 30V for 1h then at 100V for 1h. Gels were electrotransferred (Biorad) on a immobilon-PSQ membrane (Millipore) at 10V, 4°C, in a buffer containing 25 mM Tris pH8.3, 192 mM Glycine, 0.25% SDS, 20% ethanol. Membrane were blocked with 5% milk, 1X PBS, 0.5% tween20, 2h at room temperature. The HspA protein, the outer membrane protein (OMP), as well as the fusion protein A1-SPA were detected with rabbit polyclonal antibodies anti-HspA (1:500 in blocking buffer, gift of Hilde de Reuse, Pasteur Institut), and mouse monoclonal anti-OMP antibody (1:50, LSBio LS-C102923) and anti-FLAG M2 antibody (1:800, clone M2, Sigma-Aldrich). Goat anti-rabbit IgG-Horseradish Peroxydase (HRP) (1:10000, Sigma) and anti-mouse IgG-HRP (1:10000, Santa Cruz) were used as secondary antibodies and the detection was achieved with the Immobilon Western reagent (Millipore) using the ImageQuant LAS 4000 (GE-Healthcare) apparatus.

2.6 Materials.

Peptide AapA1 was synthesized by Bachem® AG (Bubendorf, Switzerland) using classical solid phase synthesis (SPPS), the peptide is elongated starting from the C-terminus to the N-terminus of the sequence, Peptide Aap1 V26A was synthesized by Twenty first Century Biochemicals® (Marlboro, MA). This synthesis is followed by standard analytical package including mass spectrometric analysis and amino acid analysis. The purity of the peptide determined by RP-HPLC was superior to 95 %. Dodecyl phosphocholine (DPC), 1,2-Dioleoyl-sn-glycero-3-phosphocholine (DOPC), Cholesterol, 1,2-Dioleoyl-sn-glycero-3-phosphoethanolamine (DOPE), 1,2-Dioleoyl-sn-glycero-3-phospho-rac-(1-glycerol) (DOPG), were purchased from Avanti Polar Lipids® (Alabaster,

AL). Materials. 1,2-dimyristoyl-sn-glycero-3-phosphoethanolamine (DMPE), 1',3'-bis[1,2-dimyristoyl-sn-glycero-3-phospho]-sn-glycerol (CL) and 1,2-dimyristoyl-d_{54}-sn-glycero-3-phospho-(1'-rac-glycerol) (DMPG-d_{54}) were purchased from Avanti Polar Lipids (Alabaster, AL). Deuterium depleted water was obtained from Eurisotop (France). Ultrapure water with a nominal resistivity of 18.2 MΩ.cm (MilliQ, Millipore, France) was used for lyophilization.

2.7 Plasmon Waveguide Resonance.

PWR (Proterion Corp. Piscataway, NJ) spectra were produced from a polarized CW laser (HeNe; λ= 632.8 and 543.5 nm). The prism are coated with SiO2 on top of a thin metal film (Ag) producing a spectral angular resolution of 1 mdeg. Two simple lipid model systems were used to mimic the eukaryotic and bacterial membrane corresponding to DOPC/DOPE/Chol (2/1/1.5 mol/mol/mol) and DOPE/DOPG (7/3 mol/mol) respectively. After the formation of the planar lipid bilayer by the Montal & Mueller method that has been thoroughly described previously [29] and after its stabilization, increasing amounts of peptide were added to the PWR cell sample with concentrations from the pM to the µM range. For each peptide addition the changes in the PWR spectra were followed for both polarizations, and we waited for the stabilization of the signal prior to the subsequent peptide addition. At the end of each experiment, the total amount of peptide in the cell reached a concentration superior to that of peptide bound to the membrane. The affinity constant were determined by following the changes in the resonance minimum position for each peptide concentration point, data was plotted and fitted by an hyperbolic function that describes the binding of a ligand to a receptor (GraphPadPrism), providing the dissociation constants: Y= (Bmax X) / (Kd+X). Bmax represents the maximum concentration bound, and Kd is the concentration of ligand required to reach half-maximal binding [30] Data fitting allowed the determination of an apparent dissociation constant for the process that comprises both peptide/lipid interaction and the lipid reorganisation that takes place to accommodate such interactions.

2.8 Circular Dichroism.

Far-UV CD experiments were recorded on a J-815 spectropolarimeter with a Peltier unit (Jasco, Tokyo Japan). Spectra were acquired at 303 K with a response time of 1 s and a step resolution of 0.5 nm with a scanning speed of 50 nm/min. A Quartz-Silicate cuvette with the pathlength of 0.1 cm was used. Seven spectra were averaged to obtain smooth spectra, followed by background correction. The final signal was processed with a Savitsky-Golay smoothing filter with 25 points. A diluted series of trifluoroethanol (TFE) by water was carried out in incremental steps of 10 % (v:v). A concentration of 70 µM of peptide was used at the start, prepared in 100 % (v/v) TFE in 10 mM acetic Acid, 1 mM DTT and 10 mM NaCl, and diluted by the same buffer without TFE at each steps. For micelle experiment, CD spectra were measured for a 70 µM of peptide in a ratio of 1:60 (mol:mol) with DPC, which corresponds to a ratio of one peptide for one micelle according the aggregation number of DPC and its CMC of 1.1 mM. The solution was sonicated for 5 min and then equilibrated for 15 min in 303 K before the measurement. A buffer consisting of 10 mM acetic acid, 1 mM DTT and 10 mM

NaCl was used. The pH of all solution was confirmed to be 4.7 by using a PH 211 microprocessor pH meter (Hanna® instruments).

2.9 Liquid state NMR spectroscopy.

A quantity of 2 mg of AapA1 peptide, or the mutant AapA1 V26A, were dissolved in 40 % (v:v) d3-TFE containing 10% (v/v) D2O, buffered by 10 mM deuterated acetic acid, 10 mM DTT and 10 mM NaCl, in a standard 5 mm Shigemi® tube. The pH 4.7 was checked directly in the NMR tube using a PH 211 microprocessor pH meter (Hanna® instruments). All NMR spectra were acquired on a Bruker® Advance 700 MHz or 800 MHz NMR spectrometer, equipped with a TXI triple resonance 1H/15N/13C/2H and z-axis gradient standard probe for the 700 Mhz spectrometer, or cryoprobe for the 800 Mhz. Chemical shifts were referenced relative to internal H_2O. Spectra were acquired using a temperature of 303 K. TOCSY (120 ms), NOESY (250 ms) and HSQC were processed using TopSpin 3.2 (Bruker®). Self-diffusion coefficients were measured at 303 K by acquiring a series of 12 pulsed-gradient stimulated echo spectra with variation of gradient strength from 10% to 90%. DOSY were processed using DOSYToolbox software [31]. The peptide molecular weight was calculated using the viscosity of 40% TFE as previously described [32]. The resonance assignments of each amino acid were identified by their distinct spin systems in 2D ^{1}H-^{1}H homonuclear experiments NMR spectra. The scalar connectivity between NH, Hα and side chain protons were established by TOCSY spectra. This process was followed by main chain directed amino acid sequence analysis, involving the identification of inter-residue NH-Hα-Hβ patterns which characterize secondary structure elements and use consecutive NOE links to assign several previously unassigned residues. The Hα-NH crosspeaks in the TOCSY were recorded with mixing times of 80 and 120 ms, and all were assigned to individual residues, except for the Hα chemical shift of residues Met-1, Asn-8 and His-5. Finally, sequential assignments were obtained from NOESY spectrum recorded with a mixing time of 50 and 250 ms.

2.10 Solid-state NMR spectroscopy:

1,2-dimyristoyl-sn-glycero-3-phosphoethanolamine (DMPE), 1',3'-bis[1,2-dimyristoyl-sn-glycero-3-phospho]-sn-glycerol (CL) and 1,2-dimyristoyl-d54-sn-glycero-3-phospho-(1'-rac-glycerol) (DMPG-d54) were purchased from Avanti Polar Lipids (Alabaster, AL). Deuterium depleted water was obtained from Eurisotop (France). Ultrapure water with a nominal resistivity of 18.2 MΩ.cm (MilliQ, Millipore, France) was used for lyophilization. To prepare the multilamellar vesicle (MLV), DMPE, DMPG and CL were mixed with or without the appropriate amount of AapA1 powder and adjusting the lipid/peptide ratio (50/1) in organic solvent (chloroform/methanol, 2:1). The solvent was evaporated with a vacuum pump to obtain a thin lipid film. Lipids were rehydrated with Ultrapure water before lyophilizing. The lipid powder was then hydrated with the appropriate amount of deuterium depleted water (75 % hydration ratio) and homogenized by 3 cycles of shaking in a vortex mixer, then freezing (liquid nitrogen, -196°C, 1 min) and finally thawing (40°C in a water bath, 10 min). This protocol leads to a milky suspension of micrometer size MLV. 2H NMR experiments were carried out using Bruker Avance II 500 MHz WB (11.75 T). 2H NMR experiments on 2H-labeled DMPG were performed at 76

MHz with a phase-cycled quadrupolar echo pulse sequence (90°x-τ-90°y-τ-acq). Acquisition parameters were as follows: spectral window of 250 kHz for 2H, π/2 pulse width of 2.62 μs, interpulse delay τ was of 40 μs, recycled delay of 1.5 s. 2k scans were used for 2H NMR. The spectra were processed using a Lorentzian line-broadening of 400 Hz for 2H spectra before the Fourier transform from the top of the echo. Samples were equilibrated for 30 min at a given temperature before data acquisition. Bruker Topspin 3.2 software was used for spectra processing. Spectral moments were calculated for each temperature using the NMR Depaker 1.0rc1 software (Copyright (C) 2009 Sébastien Buchoux).

2.11 Structure calculation.

Peak volumes of manually assigned NOESY spectra were converted by ARIA into distance restraints using the built-in distance method with a minimum distance correction of 1.8 Å and a maximum distance correction of 6.0 Å. All intra-residue restraints were discarded and only inter-residue restraints were used for structure calculation. Additionally, φ and ψ angle restraints were obtained using $^{15}N^{H}$, $^{1}H^{N}$ and $^{1}H^{a}$ chemical shifts with the program TALOS [33]. Both NOEs and dihedral-angle restraints were used as experimental input for the simulated annealing structure calculation method using the ARIA/CNS software package [34]. A total of 8 iteration steps were performed with a total of 2000 structures calculated in the last iteration. The 15 lowest-energy structures were submitted to a molecular dynamics simulation in presence of water for final refinement. The network anchoring filter was used for the four first iterations and then discarded. The dynamics protocol used a Cartesian model with steps of 0.005 ps with two intermediate cooling temperatures from 2000 K to 1000 K with 5000 steps and from 1000 K to 50 K with 10000 steps. All data processing and molecular graphics analyses were performed with UCSF Chimera package [35].

2.12 Molecular Dynamics.

Three independent MD simulations were conducted at 20 °C. Simulation (A) was run for 204 ns and consisted of 144 POPC lipids and 2 AapA1 peptides that were separated as far as possible and oriented parallel to each other in a membrane spanning fashion. Simulation (B) was run for 168 ns and had the same composition but with both peptides outside of the bilayer, which was oriented parallel to the membrane surface. Simulation (C) was run for 402 ns and featured the same peptide orientation but the membrane consisted of 112 POPC and 28 POPG molecules. Peptide structures were experimentally determined in a TFE:water mixture and simulation setup followed published procedures [36]. To neutralize the systems, 0.1 M KCl was included. The program NAMD [37] was employed for the simulation under conditions of normal pressure (1.013 bar), using the most recent CHARMM all-H C36 lipid force field [38]. This allowed for a flexible surface area during the simulation and therefore enabled the system to adapt to peptide binding (no additional force was applied in the plane of the membrane). The smooth particle mesh Ewald algorithm [39] was used to compute the electrostatic forces and the SHAKE algorithm [40] was used to keep rigid all bonds that involve hydrogen atoms, allowing for a 2 fs time step.

3 RESULTS

3.1 The small protein AapA1 targets the H. pylori inner membrane in vivo

In a previous work, we have shown that the expression of the AapA1 small ORF in *H. pylori* leads to bacterial growth arrest, and cell death without cell lysis (24). In contrast to most of the toxins belonging to type I TA systems, AapA1 displays a poor hydrophobicity index (25). To further investigate the mode of action of this small protein, we decided to monitor the subcellular localization of the AapA1 toxin in *H. pylori*. Since the generation of antibodies against this small protein failed despite several attempts, we used the sequential peptide affinity (SPA)-tag that has previously been used to detect small membrane proteins in *Escherichia coli* (Fig. 1A) [7]. This tag contains the calmodulin binding peptide followed by a repetition of 3X-FLAG. The tag has high sensitivity, and also facilitates the detection of small proteins since it adds 8 kDa to the molecule. The DNA fragment encoding the AapA1-SPA recombinant protein was cloned into the IPTG inducible vector as previously described (24). We only managed to add the SPA-tag at the C-terminus (C-ter), since attempts to add this tag at the N-terminus (N-ter) of the AapA1 toxin always resulted in frameshift mutations to create premature stop codons. However, the addition of the SPA tag at the C-ter abolished the toxicity of this recombinant protein when compared to the wild-type AapA1 toxin under the same conditions (Fig. 1B). These results suggested that the addition of the tag at the C-ter may perturb the structure adopted in this region, which could play a key role in AapA1 toxin activity. Nevertheless, we managed to detect the expression of this fusion protein by Western Blot analysis (Fig. 1C). To examine the subcellular fractionation of the C-terminally SPA-tagged AapA1 toxin, we used a protocol previously described for *H. pylori* membrane preparation (26). Most of the AapA1-SPA fusion protein was found in the membrane fraction with a small amount in the soluble part (Fig. 1C). As controls, the cytoplasmic and membrane fractions were probed with the antibody against the chaperone HspA and a porin of 19 kDa (OMP), respectively. Although the separation of the inner and outer membrane of *H. pylori* was difficult to distinguish, we observed no peptide in the outer membrane fraction (Fig. 1D), indicating that the AapA1 toxin is likely interacting with the inner membrane of *H. pylori*.

3.2 AapA1 displays high affinity to membranes and perturbs their organization

Plasmon waveguide resonance (PWR) and solid-state NMR experiments were carried out to investigate the interaction between AapA1 and model lipid bilayers. The PWR method allows for the determination of affinity constants between the peptide and the lipid bilayer, as well as information regarding mass and anisotropy changes in the lipid system. This is possible because the formed lipid bilayers are oriented relative to the incident light, and also because PWR allows resonances to be obtained with both p- (perpendicular) and s- (parallel) polarized light [41]. The method has

successfully been used to follow both protein structural changes, protein-protein interactions and peptide-lipid interactions [42, 43]. The formation of the lipid bilayer leads to positive shifts in both polarizations due to the deposition of material (lipid) in the plasmon-generating surface, and therefore an increase in the mass and refractive index. Such shifts are larger for p- than for s-polarized light, reflecting the formation of an anisotropic structure composed by the lipid bilayer, with the longer molecule axis laying perpendicular to the plasmon resonating media [44]. Successive addition of AapA1 to a eukaryotic membrane model composed of DOPC/DOPE/Chol [45] leads to an increase of negative shifts in the *s*-polarized light up to -28 mdeg (Fig. 2A). No shifts in the *p*-polarization component were observed. Peptide addition to a membrane should result in a positive shift in the spectra if the peptide only adsorbs on the surface without modifying the lipid properties as it should increase the mass of the proteolipid system (increase in refractive index that is translated by positive spectral shifts). Therefore, PWR experiments showed that the decrease in the resonance angle position must result from peptide-induced lipid reorganization. In order to test this observation, we performed deuterium (^{2}H) solid-state NMR experiments to qualitatively investigate the effect of AapA1 on liposomes constituted by lipids mimicking the *H. pylori* membrane composition [46, 47]. Liposomes made of 1,2-Dimyristoyl-sn-glycero-3-phosphorylglycerol (DMPG, deuterated), 1,2-Dimyristoyl-sn-glycero-3-phosphoethanolamine (DMPE) and cardiolipin (CL) were prepared at a molar ratio of 1:2:1 with a peptide:lipid ratio of 1:50. We used solid-state ^{2}H NMR experiments to study the effect of AapA1 on the lipid organization of the liposomes. We measured deuterium (^{2}H) quadrupolar couplings of ^{2}H-DMPG in DMPG/DMPE/CL liposomes (Fig. 2 B) in the presence and absence of AapA1, to examine the motional amplitudes of acyl chains as a function of the AapA1 insertion. The C2 methylene group gives the maximum coupling value, as it is restricted in terms of motion due to the presence of the nearby glycerol moiety, while the methyl group at the end of the acyl chain gives the smallest coupling. In the presence of the AapA1 peptide, the DMPG/DMPE/CL membrane exhibits a decrease of the orientational disorder for the twelve first carbon positions of the acyl chain, a typical behaviour for membrane peptide insertion. The order parameter of the methyl group (C14) and the methylene at C13 is not significantly changed in presence of AapA1, due to their intrinsic mobility in the bilayer. Altogether, the solid-state NMR results are in line with PWR experiments. Both methods clearly indicate that the interaction of AapA1 with a lipid bilayer changes the lipid-dynamic organization. In the PWR experiments with a slightly different bilayer composition (DOPC/DOPE/Chol), a decrease in mass may result either from an increase in the lipid surface area (which will increase the mass/area) accompanied by a flow of lipid into the plateau Gibbs border (lipid reservoir presented in the type of bilayer used), or by the formation of holes or pores in the membrane by a detergent-type effect of the peptide on the lipids. To distinguish between these two possibilities, membrane integrity measurements are necessary. We have performed a graphical analysis of the spectral changes observed in PWR experiments [48] upon peptide addition to the membrane, and found that 70% of the spectral changes result from mass changes in the membrane and 30% from structural changes. Additionally, a large decrease in the spectra depth is observed for both polarizations indicating a thinning of the lipid membrane. Such a phenomena has already been reported to occur for antimicrobial peptides [49]. Finally, apparent dissociation constants for the

interaction of AapA1 with this DOPC/DOPE/Chol membrane model were determined using PWR spectroscopy, by plotting the equilibrium resonance minimum position of the spectra for each incremental peptide addition as a function of the peptide concentration in the cell. Such apparent dissociation constants reflect both the P/L interaction as well as the lipid reorganisation that occurs to accommodate such interaction. This value was obtained only with the s-polarized light, as no overall shifts were obtained with the p-polarized light, leading to an apparent K_D value around 800 nM (Fig. 2A). Similar studies were performed with a bacteria membrane mimic composed of DOPE/DOPG (7/3 mol/mol) [45]. The results obtained were quite different compared to those obtained with the eukaryotic membrane model (DOPC/DOPE/Chol). Spectral shifts were observed with both polarizations, both negative and of similar magnitude (about -12 mdeg for both polarizations) and smaller than those obtained with the eukaryotic membrane model (-28 mdeg for *s*-pol; no shift for *p*-pol). Graphical analysis of the results attribute about 50% of the spectral changes induced by peptide addition to the bilayer to mass changes and about 50% to structural changes. Again, the decrease in mass could be ascribed to lipid removal from the bilayer and/or reorganization and will need further investigation. It is interesting to note that here, in comparison with the eukaryotic membrane, smaller changes in membrane thickness are induced by AapA1. The apparent dissociation constant obtained here is much stronger than that obtained with the eukaryotic membrane model, 25 nM (Fig. 2C), which may be explained by the establishment of electrostatic interactions, between negatively charged DOPG lipid headgroups from and positively charged residues in the peptide.

3.3 The AapA1 toxin adopts an alpha helical conformation

The secondary structure of the AapA1 peptide in a membrane mimicking environment was first explored using circular dichroism (CD) spectroscopy. In order to probe its folding within a membrane model, we used a micelle composed of DPC/SDS mixture as a simple membrane mimicking interface. This type of interface has broad use in liquid state NMR due to an intrinsic fast correlation time within the NMR time scale limits [11, 42].. The addition of SDS to AapA1/DPC micelle complexes decreased the minimum in the CD spectra at 214 nm without disturbing the β–strand signal (Fig. S1A). Acquisition of NMR spectra showed a line-broadening of peaks under these conditions (Fig. S1B) probably from the multiple unfolded conformers. We estimate that only 30-40 % of protons could be identified. An assignment of the ten first residues was completed by a sequential walk in the NH and Hα region (Fig. S1C). To optimize the structural studies by NMR at high concentrations (1 to 2 mM), we carried out screening tests at different TFE/water ratios mixtures for AapA1, which is a solvent that have been extensively used to mimics the apolar environment inside the membrane bilayer and enables at the same time the acquisition of high resolution liquid state NMR spectra (Fig. 3A). We looked for a minimal ratio of TFE, which prevents aggregation and precipitation in the NMR tube. Although TFE is known to induce an α-helix structure for hydrophobic peptides, we nevertheless found that it was the only solvent with the capacity to prepare a liquid state NMR sample. The CD spectra at 100 % TFE displayed two minima around 209 and 222 nm, characteristic of well-defined α-

helix structure. Towards 20 % TFE, these two minima disappear and pass over a shallow minima that could be the indication of mixture of β-strand and α-helix structures, finally forming a well-defined minimum around 218 nm, indicating the conversion to a β-strand/sheet structure (Fig. 3A). We however found that at 20% TFE we still observe small aggregates and broad NMR peaks. To reduce problems related with peptide aggregation, we decided from the CD and 1D ^{1}H NMR profile to study the peptide in 40 % TFE, 10 mM acetic acid, 10 mM NaCl, 2 mM DTT at pH 4.7 (Buffer A). Under these conditions, the peak dispersion and linewidths in the NOESY spectra of AapA1 peptide were optimised for structure calculations (Fig. S2). Diffusion order spectroscopy (DOSY) was used to assess the oligomer state of AapA1. We used the viscosity and the density parameter of 40 % (v:v) TFE/water solution at 303 K as 1.31 10^{-3} kg m^{-1} s^{-1} and 1.107 g cm^{-3}, respectively [50]. Experiments were carried out with peptide concentrations ranging from 40 µm to 1 mM. The DOSY experiment using the peak of the tryptophan imino proton (Fig. S3A) led to a diffusion value corresponds to a spherical object of 4161 ± 400 Da and 4500 ± 400 Da respectively. The difference from the theoretical value of 3.5 kDa of AapA1 is supported by the fact that the peptide in buffer A does not behave as a spherical object and includes the hydration shell as expected. Nevertheless, the peptide seems to be predominantly in the monomeric state (Fig. S3B and S3C). The monomeric state of AapA1 in buffer A was confirmed by native electron spray ionization mass spectrometry (Fig. S4). For structural calculations, we used conditions described above where the peptide exists mostly in a monomeric state. Briefly, from the NOESY and TOCSY spectra in buffer A, we identified all thirty residues, the connectivity pattern for the entire sequence was identified with additional support from ^{1}H-^{15}N HSQC spectra (Fig. S5). Regular secondary structure elements are obtained from a qualitative analysis of the chemicals shifts in reference to those of random coils [51]. All NOEs types that define an α-helix can be found from Ser-9 to Leu-28. Taken together, the NMR spectra indicate that AapA1 peptide adopts an α-helical conformation. The 3D structure was calculated with distance restraints obtained from a series of NOESY spectra using the ARIA/CNS software package [52, 53]. Starting from 230 unambiguous, 90 ambiguous distance restraints and 42 dihedral angle restraints derived from chemical shift analysis with Talos [33], the 3D structure was calculated and is represented in (Fig. 3B). The results reveal that AapA1 peptide consists of a helical segment spanning Ser-9 to Leu-28, with an unfolded N-terminus.

3.4 The AapA1 toxin adopts a stable transmembrane alpha helical conformation

Considering the high-resolution NMR structure of AapA1 and our biophysical results on the peptide insertion into membranes as seen by PWR and solid-state NMR, we decided to perform MD calculations to examine the structural organization of the peptide in a lipid environment. Based on the AapA1 structure solved in TFE:water mixture, we carried out MD simulations in three different sets of experiments, each containing two separated molecules of the AapA1 peptide. Both molecules were placed apart from each other in the following pre-equilibrated lipid systems: traversing a membrane of POPC (A), in the buffer surrounding a bilayer of POPC (B) or in the buffer surrounding a bilayer of a POPC:POPG (1:4 mol/mol) mixture (C). In the first case (A) we did not observe an interaction

between both peptides present in the simulation box, and they remain stable in this environment without large positional-fluctuations due to lower mobility of peptides when inserted in a bilayer. For long periods over the entire MD run, we can observe some phospholipid head-groups that establish interactions with peptide residue side chains, especially with Lys-16 and Lys-23. At many snapshots during the 200 ns simulation, these interactions with basic residues led to the immersion of the phospholipid head-groups. This immersion often shortened the distance between the leaflet head groups to 15 Å, in comparison to the average inter-leaflet distance to 37 ±4Å at positions remote from the peptide (Fig. 3C). Those interactions eventually led to an invagination of some lipid head-groups, thus inducing a phenomena of membrane thinning, The thinning of membranes due to Lys side chain interactions with phospholipids head-groups is well documented in the literature [54-56] and helped to explain why certain peptides can induce the formation of transient pores and other effects.

In the MD simulation (B), both peptides start to interact with each other after the first ~40 ns and then both peptides remain together for the rest of the simulation. During that simulation, AapA1 stayed close to the surface of POPC and did not insert across the membrane. The two peptides stayed loosely connected to the polar head-groups of POPC by electrostatic interaction between the positively charged residues with the negative charge of phosphate POPC. The MD simulation also shows that both peptides interact with each other by the apolar C-ter part, through the valine hydrophobic stretch at the end of the peptide (Fig. S6). A few typical snapshots are shown in (Fig. S6 (b)-(e)). Black arrows indicate direct interactions between POPC headgroups and peptide residues such as Tyr14, Ser18, Cys22, Lys29 and Arg30. Pink dashed circles emphasize the hydrophobic interaction between both peptides, mostly by alanine, leucine and isoleucine (displayed in green), and by valines (red). Another interesting feature is that direct H-bonding between both peptides and POPC head groups are scarce, and often with no more than one pairwise interaction per frame (1 ns).

In the case of MD run (C), (Fig. S6 (f)-(h)), both peptides quickly adsorb to the membrane surface where they interact with each other after a few ns but in a manner a little bit differently from what was observed in case (B), e.g, they remain entirely and almost always bound and adsorbed to the membrane surface. During the entire run (402 ns) both peptides established more individual contacts with the membrane and for longer periods of time. When we inspect the number of direct H-bonds between both peptides and the lipid head groups, we often find ten or more lipids from both species directly bound to the peptides. Compared with the neutral POPC membrane-model (B), the POPC:POPG mixture (run C) seems to induce some sort of competition between peptide-lipid and peptide-peptide interaction that better solubilizes the peptide in the membrane surface, in detriment of peptide-peptide interactions. This is not at all surprising since besides the negative charge from the head group, the anionic lipid offers more H-bond acceptor/donor groups. In Fig. S6 (g) we can observe a representative contact between both peptides that differs from the interaction observed in POPC exclusively.

3.5 Structural insights into AapA1 toxicity

Our structural and biophysical observations indicate an amphipathic α-helix within AapA1 that contains a hydrophobic patch responsible for the phenomena of aggregation observed during sample manipulation. According to the structure of the AapA1 peptide calculated in this work, we can subdivide the peptide into three parts; a disordered part (D) covering the first eight unfolded residues, the helical segment (H) spanning from Ser-9 to Leu-28 and finally the C-ter (R) comprising the charged amino acids Lys-29 and Arg-30 (Fig. 4A). Along this architecture, we introduced point mutations and truncations in the native peptide that extend over its natural unmodified Met-1 to its terminal Arg-30 residue. To explore which domain was required for toxicity, we produced various constructs expressing truncated peptides that are deleted either for the N-terminal part (9-30) or deleted for the two last residues (1-28) (Fig. 4A). The toxicity of these various truncated peptides was assessed in liquid growth-media after overexpression of each peptide in *E. coli* (Fig. 4B). We noted that the toxicity of the peptide is still present for a shortened sequence 9-30 which contains both H and R domains. Both constructs 1-28 and 9-28 missing the R domain do not display the toxicity effect over the cellular growth after peptide overexpression by induction with IPTG. Our results indicate that both C-ter residues, e.g., Lys-29 and Arg-30 in domain R, are crucial for toxicity, while the first 8 amino acids (observed as unstructured in the NMR structure) of domain D are not. These observations are consistent with the consensus sequence obtained with 166 AapA sequences from 91 *H. pylori* strains (Fig. S7). The consensus sequence displays a non-conserved pattern in the N-terminal region compared to the highly conserved central and C-terminal part of the peptide. We then decided to further characterize this highly conserved helical part by testing the contribution of each conserved amino acid using an alanine scanning mutagenesis approach. Each residue from Ser-9 to Leu-28 in domain H was substituted by an alanine. The results are shown in Fig. 4C. Each strain expressing a mutant peptide was plated under inducing conditions on LB plates containing IPTG. The plating scheme follows a projection of the helical wheel representation of the last 20 residues of the AapA1 peptide. As expected, a transformed strain with an empty vector (ctrl) produce large colonies at the center of the plate (Fig. 4C). Our alanine scanning analysis correlates very well with the sequence logo obtained after aligning all AapA toxins predicted in *H. pylori* (Fig. S7). With the exceptions of Ser-9 and Leu-13, each single-alanine substitution that alters the toxicity of the AapA1 peptide corresponds to the most conserved positions (i. e. positions 10, 14, 16, 19, 21 and 23). These results clearly indicate that these amino acids are crucial to maintain the function of the toxin. They define two conserved faces shown in red and green in the helical wheel representation (Fig. 4C) and in the structural modeling of the helical part of the toxin (Fig. 4D). In contrast, a hydrophobic surface appears on the opposite of these two faces. Indeed, the replacement of different hydrophobic residues (Leu-13, Iso-17, Leu-20, Val-24, Leu-27, and Leu-28) by alanine did not alter the toxicity of the peptide significantly. In line with these findings, the alanine substitution of Leu-15 or Val-26, displayed on the red face of the peptide, produces a non-toxic isoform. The predominance of somewhat larger hydrophobic residues must play a key role in peptide aggregation and toxicity, as the mutation to smaller hydrophobic residue such as Ala, produces samples that do not aggregate in water-based solutions and trigger a non-toxic phenotype (Fig. 4). This striking result led us to structurally characterize the V26A mutant. We used the same conditions reported previously for

AapA1, and by visual observation, the V26A peptide seems to aggregate much less than AapA1. The lack of aggregation was also confirmed using light scattering (data not shown). Moreover, using CD spectroscopy we remark that in buffer A the CD spectra profile of V26A presents the shape of an α-helix with the two characteristic minima as opposing to AapA1 in the same buffer conditions (Fig. S8). Using NMR spectroscopy, we inspected the chemical shift of NH cross peaks in 2D ^{1}H-^{15}N HSQC spectra to follow chemical shift perturbation in the mutant V26A related to structural changes from the wildtype (Fig. S9 and S10). We observed that Leu-27 and Lys-23 shows the highest perturbations (Fig. S10A). The i+1, i-3 residue connectivity's variations are used as indication for secondary structure α-helical formation. The assignment of the NOESY spectra were carried with the same starting point, e.g. the same pattern of sequential walking of AapA1 V26A compare to AapA1 (Fig. S11). However, the better quality of the sample leads to a greater number of well resolved cross peaks. Approximatively twice the number of distance restraints are obtained from AapA1 V26A than AapA1 spectra (compare Fig. S11A with Fig. S11B). Numerous NN (i; i+2) and αN (i; i+2) that were missing in AapA1 NOESY spectrum are present in the AapA1 V26A. The residue interaction matrix displays similarly to AapA1 with a typical α-helix pattern confirmed by the structure calculated. The α-helix starts at Ser9 and continues to Leu28, with the first N-ter residues are in an disordered state (Fig. S11B). Concerning the charged residues, AapA1 V26A is less toxic but shares the same charge distribution as the wildtype, suggesting that if the charge is essential it is not the only determinant in the observed AapA1 toxicity.

---

4 DISCUSSION

In this work, we conducted biological and biophysical experiments on the AapA1 peptide that belongs to a large family of TA systems recently discovered in *H. pylori* [27]. The goal was to decipher the mechanistic interaction of AapA1 to membranes, and to characterize the structural basis of its toxicity.

4.1 AapA1 binds to lipid membranes with high affinity and perturbs lipid organization

The AapA1 toxin tagged with the SPA shows *in vivo* a strong localization at the inner membrane of *H. pylori*. Although this peptide has a poor hydrophobic index, AapA1 binds *in vitro* to lipid model membranes mimicking both eukaryotic cells and bacteria with high affinity (800 and 25 nM, respectively) although with over 30 fold higher affinity to the bacteria membrane mimic. In both membrane-model systems, the peptide leads to perturbation of lipid organization with a decrease in lipid membrane packing and/or formation of small pores. The results are in agreement of what was observed by SSNMR and MD simulations. The peptide penetrates the membrane leading to a lipid re-organization and thinning of the bilayer in the vicinity of the peptide. The membrane thinning is also evidenced by PWR. This process is common to the mode of action of many membrane active

peptides as antimicrobial and cell penetrating peptides [57] and could be the first stage in stronger membrane perturbation (rupture, pore formation, etc). Although different properties in peptides can induce various mechanisms of membrane interference and disruption, the role or Lys and Arg residues are more in agreement with the MD results. The behaviour of Lys and Arg side chains in lipid membranes is well documented in the literature [56-58] and seems to support our results and interpretations. The importance of charged residues in other type I toxins has already been reported [11, 12, 16, 17]. It was hypothesized that positively charged residues may help targeting of the bacterial membrane that is mostly negatively charged.

4.2 The alpha helical domain of the AapA1 toxin targets the membrane of H. pylori

The three-dimensional structure adopted by the AapA1 toxin was resolved by liquid state NMR. The peptide is organized in three short segments. A short disordered N-terminal D domain, a central α-helical H domain, and the positively-charged C-ter R domain comprised only by the two critical residues Lys and Arg. MD results support a model where the peptide diffuses to a lipid membrane. The MD results support both localization of the peptide across the bilayer and adsorbed to its the surface. Unfortunately, both solid and liquid state NMR results using lipid model membranes were inconclusive due to the strong nature of aggregation of AapA1 in water-based solutions. But altogether, the results that we present here are pertinent and indicate that the α-helical part may be essential for membrane interaction as found for most of the toxins belonging to type I TA systems [4, 15]. The Fst toxin (*E. faecalis*) displays an alpha helical structure that is able to insert throughout the inner membrane [11] like SprA1 [12] and TisB [10] for example. A reorganization of the membrane bilayer is induced by AapA1, at concentrations as low as nM range, undergoing an increase in the lipid surface area and a membrane thinning. Important membrane disruption by pore formation is only observable at high concentration of peptide (≈50 µM) as suggest by haemolysis experiments (data not shown). The interaction between AapA1 and cellular membranes does not severely damage the membrane integrity as observed in different cases of toxins reported in the literature [14]. During the structural analysis of AapA1 toxin, we have shown that the D domain does not play a key role in AapA1 toxicity. It is a sub-domain of the AapA peptide, which is highly variable in sequence compared to the rest of the peptide. The Fst toxin, which belongs to Type I TA systems, has an α-helical structure resolved in DPC micelles and it has the particularity to present an unfolded C-ter part that does not interact with the micelle [11]. The N-ter segment found in AapA1 only conserves a global positively charge, while Fst conserve a global negatively charge of its unfolded part [59]. However, the conservation of this positive charge in AapA1 may be important for its interaction with a partner as hypothesized with negative charge in the case of Fst [11]. It is also possible that its existence is correlated to the sequence of the IsoA1 RNA. Indeed the first 8 amino acid codons of the peptide match to the first 24 nucleotides of the antitoxin [27].

4.3 AapA1 displays a minimal sequence for toxicity including the C-ter domain

Despite having a consensus length of 30 amino acids, we found through sequence truncation experiments that the length of this peptide can be further minimized to 22 residues while still preserving the same toxicity, and the first 8 residues that are part of the D domain can be removed without affecting toxicity. This is similar to what was previously observed in *E. coli* with the Ibs peptide which remains toxic despite multiple deletions [9]. However, the last two residues of the peptide cannot be removed without compromising the toxicity of the AapA1 toxin. It is interesting to note that all *H. pylori* AapA* toxin that are shorter than 30 amino acids have lost the charged R domain sequence (Fig.S13). A peptide consensus of 29 amino acids bearing a terminal lysine or arginine is also found in two type I toxins present in *E. coli* (i.e TisB [10] and ZorO [5]). The presence of basic residues at the C-terminal part has been demonstrated to be important for phospholipid preliminary binding [60]. The C-ter charge effect is also observed on three other type I TA toxins, such as LdrD with Arg-Lys conserved residues [61], SprA1 [62] and BsrG [63] with Lys-Lys residues, and for which a membrane toxic effect has also been reported, suggesting a crucial role of these basic C-ter residues during the toxicity process.

4.4 A specific amino acid pattern in the transmembrane domain is required for toxicity

Similar to what was shown for Ibs and Fst [9, 24], a single amino acid substitution can alter the toxicity of the AapA1 toxin. Most of these mutations are located in the α-helical H domain and correspond to the most conserved residues in all AapA peptides predicted in *H. pylori*. One of the most striking mutations is the replacement of Val-26. The absence of toxicity in AapA1 V26A is somehow puzzling since the mutant peptide retains almost the same α-helical content and charge distribution. The key elements that could explain the loss of toxicity may lie in the subtle structural differences observed after modifications of the hydrophobic patch. Alanine is less bulky, and with a global volume of Vr = 67 $Å^3$ against 105 Å3 for Valine it samples less steric clashes with other residues side chains, especially with Cys22 and Lys23 that are in the same side of the α-helix as seen from the NMR and MD results. In addition, less steric clashes allow greater side-chain mobility disfavouring peptide-peptide interactions. Corroborating this analysis is the fact that the mutant is much more easily dissolved in water (less aggregates) at equivalent concentrations than the wild type. Another indication of further intra-chain stability in detriment of inter-chain interactions could be obtained from inspection of the NOESY spectra. We observe more intra-chain cross peaks and a relative strengthening of the NH-NH cross peaks for Gly21-Cys22, Val24-Val25, Leu27-Leu28, and Trp10-Lys11. Altogether, the point mutation V26A seems to stabilize the peptide chain. However, given the similar structure of the V26A mutant with the wildtype peptide indicates that most probably the helical structure does not relate to toxicity. One hypothesis is that the AapA1 toxin instead requires a cellular partner in order to promote its activity, as observed for example with the small proteins ArcZ and MgtS [22, 64]. The other hypothesis is that the more important degree of aggregation observed in AapA1 is mechanistically important for its toxicity. This small protein might be able to form a pore similar to what has been observed for other type I toxins such as Ibs [9, 65] and TisB [10]. The short segments of AapA1 are spatially organized to give the peptide an overall ability to form multiple-order oligomers with

amphipathic character. In that case, the absence of toxicity of the AapA1 V26A mutant could be explained by a faulty or weak formation of the oligomeric form.

4.5 Comparison of AapA1 with other known type I toxins and putative mode of action

Our study has revealed that the AapA1 toxin shares many similarities with other well-studied type I TA toxins. Despite a poor sequence homology (FigS12)), AapA1 adopt a stable α-helical domain as reported for three other toxins, such as Fst, sprA1 and TisB [66], flanked by important positively charged amino acid residues. Of note, our structural data have been validated by a genetic approach carried out on the AapA3 toxin, a closely-related homolog of the AapA1 toxin [67, 68]). This *in vivo* approach, named FASTBAC-seq, has confirmed the existence of a N-ter disordered domain, a transmembrane helix domain and the importance of the two Arg-Lys residue at the C-ter of the toxin. However how does the AapA1 toxin affect the membrane integrity and mediate toxicity is yet poorly understood. Recent studies on the HokB protein has shown that this toxin can form a pore leading to proton leakage and membrane depolarisation [69] . However the HokB toxin is quite larger (52 aa) compared to most of the other described type I toxin (around 30 amino acids) (FigS12). This result strongly suggest that the HokB toxin act as an oligomer. However, we have not been able yet to detect the formation of a stable oligomer of AapA1. Alternatively, while most type I toxins appears to display common structural motifs that allow them to interact with a good affinity to cellular membranes, they may exert their toxic effect indirectly or in conjunction with other partners. The mode of action of these toxins may also follow the depolarization model by proton diffusion or transport, passive and transitory pore formation *via* a carpet mechanism, or a combination of multiple mechanisms. When peptides aggregate and at same time interact with membranes, they can also induce bundling events that disrupt the membrane. For that to happen it is not necessary to completely disrupt the membrane or induce transmembrane channel formation, but its sufficient to modify the collective properties of the membrane until it becomes unstable [70] and induces negative Gaussian membrane curvature as observed in MD simulations of AapA1. The effect is observed in a broad spectra of peptides [70, 71] with and without aggregation driven membrane protrusion.

---

5 CONCLUSION

In summary, our data show that the biophysical and structural properties of the AapA1 toxin might perturb the cellular membrane and could be used by *H. pylori* to adapt its growth in response to various environmental stresses that this bacterium encounters in the stomach. Further studies are ongoing to understand how the expression of the AapA1 toxin is regulated and in which metabolic pathway this toxin-antitoxin system is involved.

ACCESSION NUMBERS

Atomic coordinates for the reported NMR structures have been deposited with the Protein Data bank under accession number 6GIG for AapA1 and 6GIF for AapA1 V26A.

APPENDIX SUPPLEMENTARY DATA

Supplementary Data are available online

ACKNOWLEDGEMENT

We thank present and past members of the ARNA lab for helpful discussions, especially Frédéric Rosu concerning (ESI-MS) applications and Cameron Mackereth for a careful proofreading of the manuscript.

FUNDING

This work was funded in part by the INSERM, CNRS, University of Bordeaux, and ANR Bactox1 (Project ANR-12-BSV5-0025). The work on the 800 MHz NMR spectrometer (IECB) was possible thanks to support from TGIR-RMN-THC Fr3050 CNRS, CNRS UMS3033, Inserm US001, Univ. Bordeaux. Work in the Sharma lab is supported by DFG grant Sh580/8-1.

AUTHORS CONTRIBUTIONS

Conceptualization : DNK, GFS and FD; Data curation: DNK, IA, AV, AL and GFS; Formal analysis: DNK, IA, AV, AL and GFS, ; Funding acquisition: GFS, AL and FD; Investigation: DNK, IA, GFS, SC, AV and DM; Methodology: DNK, IA, AV, DM, AL, CMS and GFS; Project administration: FD; Supervision: AL, GFS and FD; Visualization: DNK, AV and GFS; Writing - original draft: DNK, IA, AL, AV, GFS and FD; Writing – review and editing: GFS and FD.

REFERENCES

[1] N. Goeders, L. Van Melderen, Toxin-antitoxin systems as multilevel interaction systems, Toxins 6(1) (2014) 304-24.
[2] A. Harms, E. Maisonneuve, K. Gerdes, Mechanisms of bacterial persistence during stress and antibiotic exposure, Science 354(6318) (2016).
[3] D. Lobato-Marquez, R. Diaz-Orejas, F. Garcia-Del Portillo, Toxin-antitoxins and bacterial virulence, FEMS microbiology reviews 40(5) (2016) 592-609.
[4] S. Brantl, N. Jahn, sRNAs in bacterial type I and type III toxin-antitoxin systems, FEMS microbiology reviews 39(3) (2015) 413-27.
[5] J. Wen, E.M. Fozo, sRNA Antitoxins: More than One Way to Repress a Toxin, Toxins 6(8) (2014) 2310-2335.
[6] N. Jahn, S. Brantl, One antitoxin--two functions: SR4 controls toxin mRNA decay and translation, Nucleic Acids Res 41(21) (2013) 9870-80.
[7] M.R. Hemm, B.J. Paul, T.D. Schneider, G. Storz, K.E. Rudd, Small membrane proteins found by comparative genomics and ribosome binding site models, Mol Microbiol 70(6) (2008) 1487-501.
[8] S.L. Grage, S. Afonin, S. Kara, G. Buth, A.S. Ulrich, Membrane Thinning and Thickening Induced by Membrane-Active Amphipathic Peptides, Frontiers in cell and developmental biology 4 (2016) 65.

[9] W.W. Mok, N.H. Patel, Y. Li, Decoding toxicity: deducing the sequence requirements of IbsC, a type I toxin in Escherichia coli, The Journal of biological chemistry 285(53) (2010) 41627-36.
[10] T. Steinbrecher, S. Prock, J. Reichert, P. Wadhwani, B. Zimpfer, J. Burck, M. Berditsch, M. Elstner, A.S. Ulrich, Peptide-Lipid Interactions of the Stress-Response Peptide TisB That Induces Bacterial Persistence, Biophys J 103(7) (2012) 1460-1469.
[11] C. Gobl, S. Kosol, T. Stockner, H.M. Ruckert, K. Zangger, Solution Structure and Membrane Binding of the Toxin Fst of the par Addiction Module, Biochemistry-Us 49(31) (2010) 6567-6575.
[12] N. Sayed, S. Nonin-Lecomte, S. Rety, B. Felden, Functional and Structural Insights of a Staphylococcus aureus Apoptotic-like Membrane Peptide from a Toxin-Antitoxin Module, Journal of Biological Chemistry 287(52) (2012) 43454-43463.
[13] I.N. Wang, D.L. Smith, R. Young, Holins: The protein clocks of bacteriophage infections, Annu Rev Microbiol 54 (2000) 799-825.
[14] M. Zasloff, Antimicrobial peptides of multicellular organisms, Nature 415(6870) (2002) 389-395.
[15] R. Brielle, M.L. Pinel-Marie, B. Felden, Linking bacterial type I toxins with their actions, Curr Opin Microbiol 30 (2016) 114-121.
[16] K. Gerdes, F.W. Bech, S.T. Jorgensen, A. Lobner-Olesen, P.B. Rasmussen, T. Atlung, L. Boe, O. Karlstrom, S. Molin, K. von Meyenburg, Mechanism of postsegregational killing by the hok gene product of the parB system of plasmid R1 and its homology with the relF gene product of the E. coli relB operon, The EMBO journal 5(8) (1986) 2023-9.
[17] N. Verstraeten, W.J. Knapen, C.I. Kint, V. Liebens, B. Van den Bergh, L. Dewachter, J.E. Michiels, Q. Fu, C.C. David, A.C. Fierro, K. Marchal, J. Beirlant, W. Versees, J. Hofkens, M. Jansen, M. Fauvart, J. Michiels, Obg and Membrane Depolarization Are Part of a Microbial Bet-Hedging Strategy that Leads to Antibiotic Tolerance, Mol Cell 59(1) (2015) 9-21.
[18] R. Weel-Sneve, K.I. Kristiansen, I. Odsbu, B. Dalhus, J. Booth, T. Rognes, K. Skarstad, M. Bjoras, Single Transmembrane Peptide DinQ Modulates Membrane-Dependent Activities, Plos Genet 9(2) (2013).
[19] K.E. Weaver, D.M. Weaver, C.L. Wells, C.M. Waters, M.E. Gardner, E.A. Ehli, Enterococcus faecalis plasmid pAD1-encoded Fst toxin affects membrane permeability and alters cellular responses to lantibiotics, J Bacteriol 185(7) (2003) 2169-2177.
[20] C. Unoson, E.G.H. Wagner, A small SOS-induced toxin is targeted against the inner membrane in Escherichia coli, Molecular Microbiology 70(1) (2008) 258-270.
[21] N. Jahn, S. Brantl, H. Strahl, Against the mainstream: the membrane-associated type I toxin BsrG from Bacillus subtilis interferes with cell envelope biosynthesis without increasing membrane permeability, Molecular Microbiology 98(4) (2015) 651-666.
[22] H. Wang, X. Yin, M. Wu Orr, M. Dambach, R. Curtis, G. Storz, Increasing intracellular magnesium levels with the 31-amino acid MgtS protein, Proc Natl Acad Sci U S A 114(22) (2017) 5689-5694.
[23] J.W. Modell, A.C. Hopkins, M.T. Laub, A DNA damage checkpoint in Caulobacter crescentus inhibits cell division through a direct interaction with FtsW (vol 25, pg 1328, 2011), Gene Dev 25(15) (2011) 1662-1662.
[24] K.E. Weaver, S.G. Reddy, C.L. Brinkman, S. Patel, K.W. Bayles, J.L. Endres, Identification and characterization of a family of toxin-antitoxin systems related to the Enterococcus faecalis plasmid pAD1 par addiction module, Microbiol-Sgm 155 (2009) 2930-2940.
[25] E.M. Fozo, K.S. Makarova, S.A. Shabalina, N. Yutin, E.V. Koonin, G. Storz, Abundance of type I toxin-antitoxin systems in bacteria: searches for new candidates and discovery of novel families, Nucleic Acids Res 38(11) (2010) 3743-3759.
[26] D.S. Coray, N.E. Wheeler, J.A. Heinemann, P.P. Gardner, Why so narrow: Distribution of anti-sense regulated, type I toxin-antitoxin systems compared with type II and type III systems, Rna Biol 14(3) (2017) 275-280.
[27] H. Arnion, D.N. Korkut, S.M. Gelo, S. Chabas, J. Reignier, I. Iost, F. Darfeuille, Mechanistic insights into type I toxin antitoxin systems in Helicobacter pylori: the importance of mRNA folding in controlling toxin expression, Nucleic Acids Res 45(8) (2017) 4782-4795.
[28] C.M. Sharma, S. Hoffmann, F. Darfeuille, J. Reignier, S. Findeiss, A. Sittka, S. Chabas, K. Reiche, J. Hackermuller, R. Reinhardt, P.F. Stadler, J. Vogel, The primary transcriptome of the major human pathogen Helicobacter pylori, Nature 464(7286) (2010) 250-255.
[29] Z. Salamon, D. Huang, W.A. Cramer, G. Tollin, Coupled plasmon-waveguide resonance spectroscopy studies of the cytochrome b6f/plastocyanin system in supported lipid bilayer membranes, Biophys J 75(4) (1998) 1874-85.
[30] I.D. Alves, S.M. Cowell, Z. Salamon, S. Devanathan, G. Tollin, V.J. Hruby, Different structural states of the proteolipid membrane are produced by ligand binding to the human delta-opioid receptor

as shown by plasmon-waveguide resonance spectroscopy, Molecular pharmacology 65(5) (2004) 1248-57.
[31] M. Nilsson, The DOSY Toolbox: a new tool for processing PFG NMR diffusion data, Journal of magnetic resonance 200(2) (2009) 296-302.
[32] R. Evans, Z. Deng, A.K. Rogerson, A.S. McLachlan, J.J. Richards, M. Nilsson, G.A. Morris, Quantitative interpretation of diffusion-ordered NMR spectra: can we rationalize small molecule diffusion coefficients?, Angewandte Chemie 52(11) (2013) 3199-202.
[33] Y. Shen, F. Delaglio, G. Cornilescu, A. Bax, TALOS plus : a hybrid method for predicting protein backbone torsion angles from NMR chemical shifts, J Biomol Nmr 44(4) (2009) 213-223.
[34] W. Rieping, M. Habeck, B. Bardiaux, A. Bernard, T.E. Malliavin, M. Nilges, ARIA2: Automated NOE assignment and data integration in NMR structure calculation, Bioinformatics 23(3) (2007) 381-382.
[35] E.F. Pettersen, T.D. Goddard, C.C. Huang, G.S. Couch, D.M. Greenblatt, E.C. Meng, T.E. Ferrin, UCSF Chimera--a visualization system for exploratory research and analysis, Journal of computational chemistry 25(13) (2004) 1605-12.
[36] S. Jo, T. Kim, W. Im, Automated builder and database of protein/membrane complexes for molecular dynamics simulations, PloS one 2(9) (2007) e880.
[37] J.C. Phillips, R. Braun, W. Wang, J. Gumbart, E. Tajkhorshid, E. Villa, C. Chipot, R.D. Skeel, L. Kale, K. Schulten, Scalable molecular dynamics with NAMD, Journal of computational chemistry 26(16) (2005) 1781-802.
[38] J.B. Klauda, R.M. Venable, J.A. Freites, J.W. O'Connor, D.J. Tobias, C. Mondragon-Ramirez, I. Vorobyov, A.D. MacKerell, Jr., R.W. Pastor, Update of the CHARMM all-atom additive force field for lipids: validation on six lipid types, The journal of physical chemistry. B 114(23) (2010) 7830-43.
[39] U. Essmann, L. Perera, M.L. Berkowitz, T. Darden, H. Lee, L.G. Pedersen, A Smooth Particle Mesh Ewald Method, J Chem Phys 103(19) (1995) 8577-8593.
[40] W.F. Vangunsteren, H.J.C. Berendsen, Algorithms for Macromolecular Dynamics and Constraint Dynamics, Mol Phys 34(5) (1977) 1311-1327.
[41] I.D. Alves, C.K. Park, V.J. Hruby, Plasmon resonance methods in GPCR signaling and other membrane events, Current protein & peptide science 6(4) (2005) 293-312.
[42] G.F. Salgado, R. Marquant, A. Vogel, I.D. Alves, S.E. Feller, N. Morellet, S. Bouaziz, Structural studies of HIV-1 Gag p6ct and its interaction with Vpr determined by solution nuclear magnetic resonance, Biochemistry-Us 48(11) (2009) 2355-67.
[43] I.D. Alves, S. Lecomte, Study of G-Protein Coupled Receptor Signaling in Membrane Environment by Plasmon Waveguide Resonance, Acc Chem Res 52(4) (2019) 1059-1067.
[44] E. Harte, N. Maalouli, A. Shalabney, E. Texier, K. Berthelot, S. Lecomte, I.D. Alves, Probing the kinetics of lipid membrane formation and the interaction of a nontoxic and a toxic amyloid with plasmon waveguide resonance, Chem Commun (Camb) 50(32) (2014) 4168-71.
[45] K. Witschas, M.L. Jobin, D.N. Korkut, M.M. Vladan, G. Salgado, S. Lecomte, V. Vlachova, I.D. Alves, Interaction of a peptide derived from C-terminus of human TRPA1 channel with model membranes mimicking the inner leaflet of the plasma membrane, Biochim Biophys Acta 1848(5) (2015) 1147-56.
[46] G. Geis, H. Leying, S. Suerbaum, W. Opferkuch, Unusual fatty acid substitution in lipids and lipopolysaccharides of Helicobacter pylori, Journal of clinical microbiology 28(5) (1990) 930-2.
[47] M. Haque, Y. Hirai, K. Yokota, K. Oguma, Lipid profiles of Helicobacter pylori and Helicobacter mustelae grown in serum-supplemented and serum-free media, Acta medica Okayama 49(4) (1995) 205-11.
[48] V.J. Hruby, I. Alves, S. Cowell, Z. Salamon, G. Tollin, Use of plasmon waveguide resonance (PWR) spectroscopy for examining binding, signaling and lipid domain partitioning of membrane proteins, Life sciences 86(15-16) (2010) 569-74.
[49] A. Mecke, D.K. Lee, A. Ramamoorthy, B.G. Orr, M.M. Banaszak Holl, Membrane thinning due to antimicrobial peptide binding: an atomic force microscopy study of MSI-78 in lipid bilayers, Biophys J 89(6) (2005) 4043-50.
[50] R. Palepu, J. Clarke, Viscosities and densities of 2,2,2-Trifluoroethanol plus water at various temperatures, Thermochimica Acta 156 (1989) 359-363.
[51] K. Wüthrich, NMR of Proteins and Nucleic Acids, Wiley1986.
[52] M. Nilges, M.J. Macias, S.I. O'Donoghue, H. Oschkinat, Automated NOESY interpretation with ambiguous distance restraints: the refined NMR solution structure of the pleckstrin homology domain from beta-spectrin, Journal of molecular biology 269(3) (1997) 408-22.
[53] A.T. Brunger, Version 1.2 of the Crystallography and NMR system, Nature protocols 2(11) (2007) 2728-33.

[54] K. Akabori, K. Huang, B.W. Treece, M.S. Jablin, B. Maranville, A. Woll, J.F. Nagle, A.E. Garcia, S. Tristram-Nagle, HIV-1 Tat membrane interactions probed using X-ray and neutron scattering, CD spectroscopy and MD simulations, Biochim Biophys Acta 1838(12) (2014) 3078-87.
[55] H.D. Herce, A.E. Garcia, Molecular dynamics simulations suggest a mechanism for translocation of the HIV-1 TAT peptide across lipid membranes, Proc Natl Acad Sci U S A 104(52) (2007) 20805-10.
[56] E.M. Cornett, N.E. Goeders, 96-hour methamphetamine self-administration in male and female rats: a novel model of human methamphetamine addiction, Pharmacology, biochemistry, and behavior 111 (2013) 51-7.
[57] D.S. Cerutti, R.E. Duke, T.A. Darden, T.P. Lybrand, Staggered Mesh Ewald: An extension of the Smooth Particle-Mesh Ewald method adding great versatility, Journal of chemical theory and computation 5(9) (2009) 2322.
[58] Y. Zhang, W. Lu, M. Hong, The membrane-bound structure and topology of a human alpha-defensin indicate a dimer pore mechanism for membrane disruption, Biochemistry-Us 49(45) (2010) 9770-82.
[59] K.E. Weaver, The Type I toxin-antitoxin par locus from Enterococcus faecalis plasmid pAD1: RNA regulation by both cis- and trans-acting elements, Plasmid 78 (2015) 65-70.
[60] D. Scheglmann, K. Werner, G. Eiselt, R. Klinger, Role of paired basic residues of protein C-termini in phospholipid binding, Protein engineering 15(6) (2002) 521-8.
[61] M. Kawano, T. Oshima, H. Kasai, H. Mori, Molecular characterization of long direct repeat (LDR) sequences expressing a stable mRNA encoding for a 35-amino-acid cell-killing peptide and a cis-encoded small antisense RNA in Escherichia coli, Mol Microbiol 45(2) (2002) 333-49.
[62] M.L. Pinel-Marie, R. Brielle, B. Felden, Dual toxic-peptide-coding Staphylococcus aureus RNA under antisense regulation targets host cells and bacterial rivals unequally, Cell reports 7(2) (2014) 424-35.
[63] N. Jahn, H. Preis, C. Wiedemann, S. Brantl, BsrG/SR4 from Bacillus subtilis--the first temperature-dependent type I toxin-antitoxin system, Mol Microbiol 83(3) (2012) 579-98.
[64] E.C. Hobbs, X. Yin, B.J. Paul, J.L. Astarita, G. Storz, Conserved small protein associates with the multidrug efflux pump AcrB and differentially affects antibiotic resistance, Proc Natl Acad Sci U S A 109(41) (2012) 16696-701.
[65] E.M. Fozo, M. Kawano, F. Fontaine, Y. Kaya, K.S. Mendieta, K.L. Jones, A. Ocampo, K.E. Rudd, G. Storz, Repression of small toxic protein synthesis by the Sib and OhsC small RNAs, Mol Microbiol 70(5) (2008) 1076-93.
[66] R. Brielle, M.L. Pinel-Marie, B. Felden, Linking bacterial type I toxins with their actions, Curr Opin Microbiol 30 (2016) 114-121.
[67] S. Masachis, N.J. Tourasse, S. Chabas, O. Bouchez, F. Darfeuille, FASTBAC-Seq: Functional Analysis of Toxin-Antitoxin Systems in Bacteria by Deep Sequencing, Methods Enzymol 612 (2018) 67-100.
[68] S. Masachis, N.J. Tourasse, C. Lays, M. Faucher, S. Chabas, I. Iost, F. Darfeuille, A genetic selection reveals functional metastable structures embedded in a toxin-encoding mRNA, bioRxiv (2019) 615682.
[69] D. Wilmaerts, L. Dewachter, P.J. De Loose, C. Bollen, N. Verstraeten, J. Michiels, HokB Monomerization and Membrane Repolarization Control Persister Awakening, Mol Cell (2019).
[70] M. Shahmiri, M. Enciso, A. Mechler, Controls and constrains of the membrane disrupting action of Aurein 1.2, Scientific reports 5 (2015) 16378.
[71] S. Galdiero, A. Falanga, M. Cantisani, M. Vitiello, G. Morelli, M. Galdiero, Peptide-lipid interactions: experiments and applications, International journal of molecular sciences 14(9) (2013) 18758-89.

FIGURE LEGENDS

Figure 1: Toxicity and cellular localization of the AapA1 peptide in H. pylori. (**A**) Schematic representation of the inducible constructs expressing either the AapA1 ORF of H. pylori 26695 strain alone (pAapA1) or fused with the SPA-tag at the C-ter (pAapA1-SPA). The two synonymous mutations inactivating the promoter (shown in grey) of the antitoxin RNA are indicated in red. (**B**) Growth curves of the strains carrying either the pAapA1 (square) or pAapA1-SPA (circle) plasmids. The addition of IPTG (1mM) is indicated by a blue star (**C**). Total protein of the strains grown in (**B**) were extracted, run into a Tricine SDS PAGE (10%) and revealed by immunoblots. Cytoplasmic and membrane fractions of the strain expressing the AapA1-SPA recombinant were further prepared by ultracentrifugation (see material and methods for details). We used anti-FLAG antibodies to reveal the expression of the C-ter SPA-tagged AapA1 toxin. Antibodies targeting the co-chaperone HspA and a porin (OMP) a served as internal controls for the cytoplasmic and membrane fraction, respectively. (**D**) The inner membrane (IN) was then separated from the outer membrane (OUT) by an additional ultra-centrifugation step in presence of N-lauroyl sarcosine 1%.

Figure 2: *In vitro* effect of AapA1 on lipid membrane models and affinity followed by Plasmon Waveguide Resonance (PWR) (A and C), solid-state nuclear magnetic resonance (SSNMR) (**B**). Effect of AapA1 followed by PWR using both *p*- (red square) and *s*- (black circle) polarized light on lipid membrane models mimicking Eukaryote (**A**) and Prokaryote (**C**) cell membranes. The affinity of AapA1 toxin for model membranes was determined by plotting the resonance minimum position as a function of concentration and fitting using a classic hyperbolic binding equation details in Material and Methods). The order parameters of the membrane along the acyl chain in presence of AapA1 were probed by SSNMR (**B**).

Figure 3: Structural study of AapA1 toxin in membrane mimicking environment. (**A**) Circular dichroism spectra of AapA1 toxin in decreasing amount of TFE. In red, the spectrum of 70 µM AapA1 in 10 mM acetic acid, 1 mM DTT and 10 mM NaCl with 40 % TFE (v:v) is shown, which are the conditions used for the structure study. (**B**) Visualization of 15 overlapped structures of AapA1 in 40 % TFE (v:v) 10 mM deuterated acetic acid, 2 mM DTT and 10 mM NaCl. RMSD values are shown for backbone atoms only and for all atoms of each residue. (**C**) Molecular dynamics snapshot of AapA1 transversally inserted in a POPC bilayer. The image was created after 107 ns and represents a typical conformation of both peptides. For the sake of clarity, the membrane of POPC is not shown, and only the phosphate groups are shown (cyan spheres). Dark-blue flat disk represents the average phosphate groups positioning in the membrane. Over the entire run we can observe some phospholipids head-groups that establish interactions with the peptides and especially with Lys-16 and Lys-23, whose side chains are separated by ~15Å. Those interactions lead to invagination of some lipid head-groups thinning the membrane as close as 15 Å, whereas otherwise the average distance is ~37 Å at places far from the peptide. Some water molecules were left in the figure in order to appreciate their insertion deep inside the bilayer.

Figure 4: The AapA1 toxin is organized in three domains. (**A**) Schematic representation of the AapA1 toxin with 3 domains: disordered (D), Helix (H), positively charged (R). (**B**) Growth curves of E. coli C43 cells expressing either truncated peptide or single amino acid substitutions. Empty squares and circles correspond to cells expressing AapA1 peptide without the two last residues (KR) at the C-terminus. Grey square and circle corresponds to cells expressing AapA1 peptide without the last R residue. Red square and circle correspond to cells expressing AapA1 with the two last KR residues. The red arrow indicates the addition of IPTG (0.25 mM). Helical wheel representation of the AapA1 peptide (left **C**) where each amino acid is represented with different size circle proportional to the bulkiness of the respective side chain. On the right depicts transformed *E. coli* culture cells with a vector expressing the toxin substituted for a single residue are plated similarly to the helical wheel projection with control cultures in the center (right **C**). In bottom panel (**D**) we can see represented the averaged AapA1 peptide structure. Red and blue surfaces represent the hydrophobic and positively charged residues respectively. The bottom insert put on evidence the amphipathic properties of AapA1 peptide. Alanine substitution disrupting the toxicity of the peptide are shown by the number of the residue in red and green surfaces, clearly forming two distinct sides of the α-helix.

Figure 1

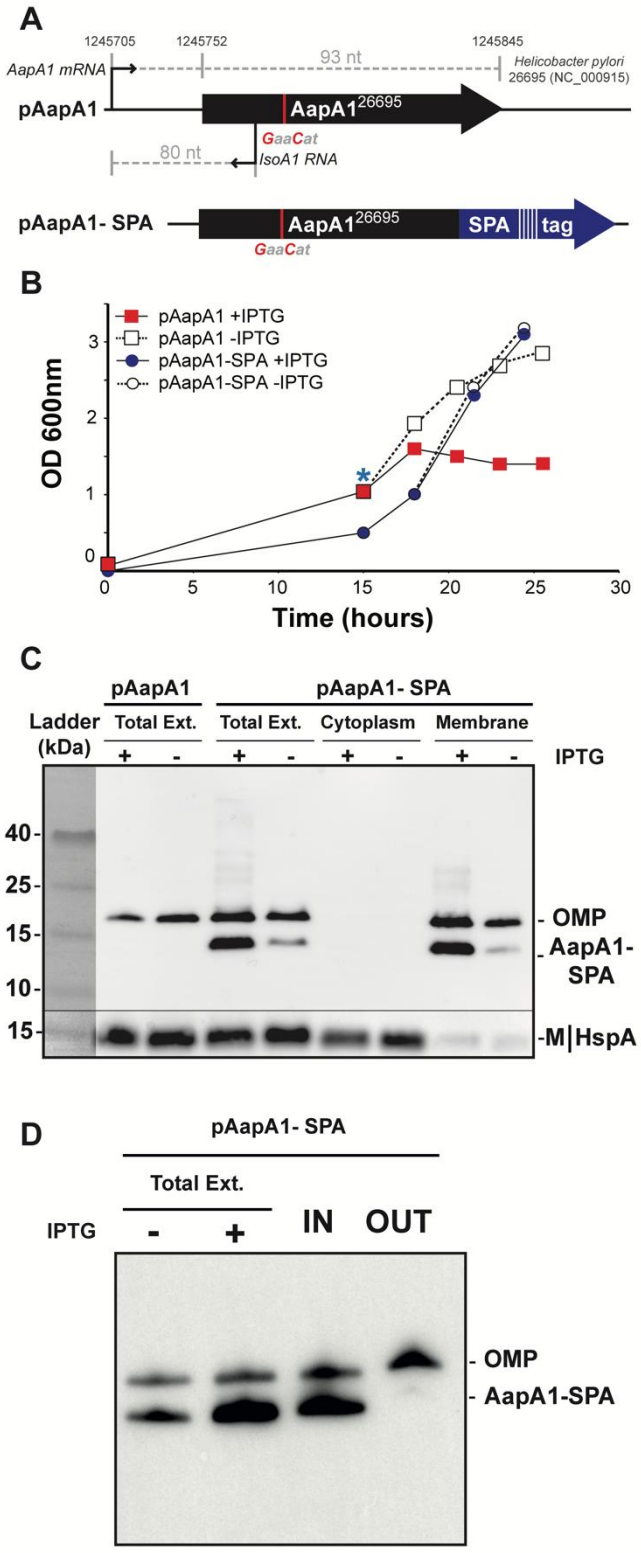
A
1245705
1245752
93 nt
1245845
AapA1 mRNA
Helicobacter pylori
26695 (NC_000915)
pAapA1
AapA1 26695
GaaCat
80 nt
IsoA1 RNA
pAapA1- SPA
AapA1 26695
SPA
tag
GaaCat
B
pAapA1 +IPTG
pAapA1 -IPTG
pAapA1-SPA +IPTG
pAapA1-SPA -IPTG
OD 600nm
Time (hours)
C
pAapA1
pAapA1- SPA
Ladder (kDa)
Total Ext.
Total Ext.
Cytoplasm
Membrane
IPTG
40
25
15
10
15
OMP
AapA1-SPA
M|HspA
D
pAapA1- SPA
Total Ext.
IPTG
IN
OUT
OMP
AapA1-SPA

Figure 2

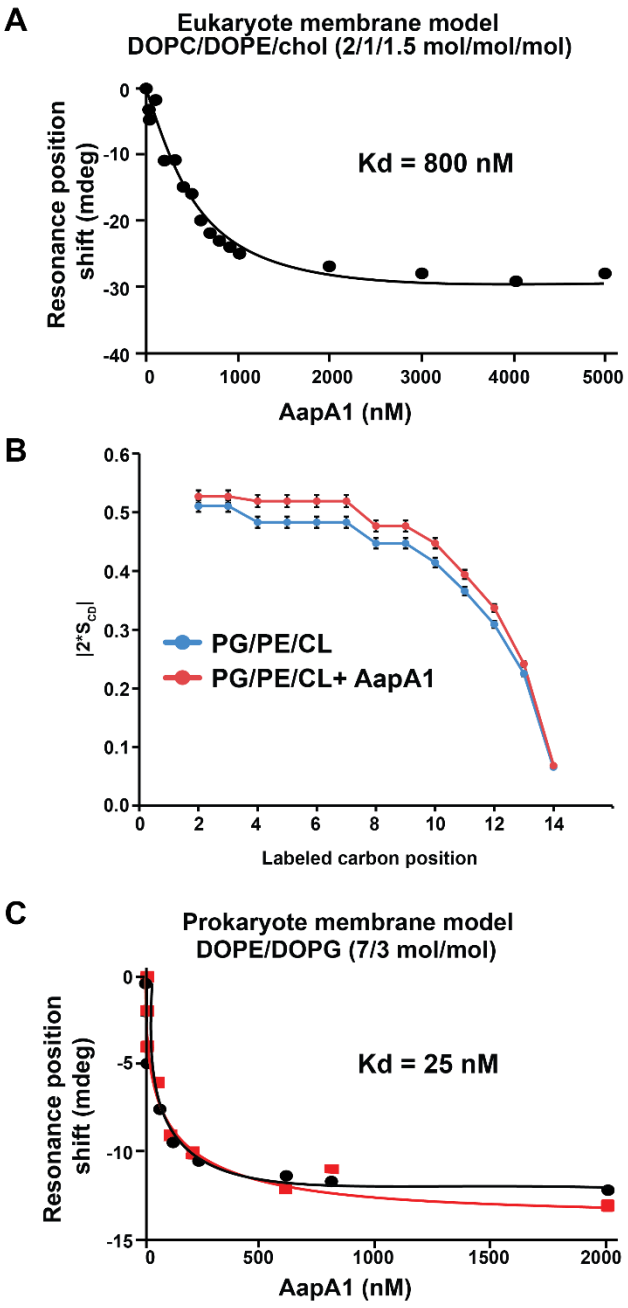
A
Eukaryote membrane model
DOPC/DOPE/chol (2/1/1.5 mol/mol/mol)
Resonance position shift (mdeg)
Kd = 800 nM
AapA1 (nM)
B
|2*S_CD|
PG/PE/CL
PG/PE/CL+ AapA1
Labeled carbon position
C
Prokaryote membrane model
DOPE/DOPG (7/3 mol/mol)
Resonance position shift (mdeg)
Kd = 25 nM
AapA1 (nM)

Figure 3

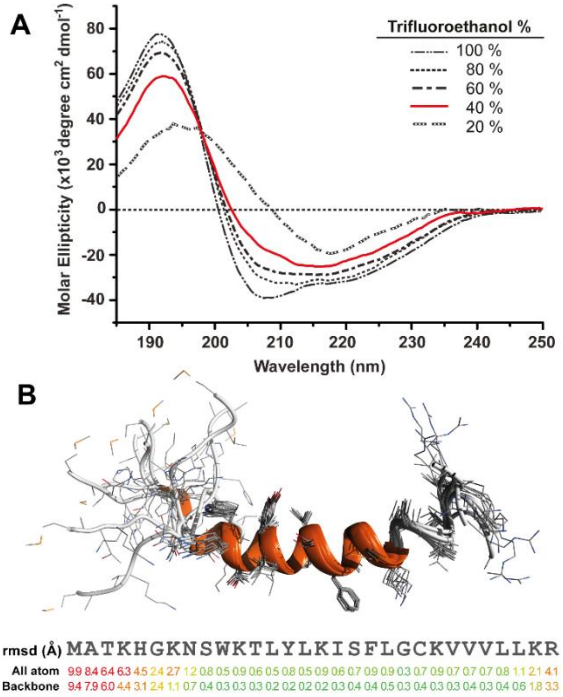
A
Trifluoroethanol %
100 %
80 %
60 %
40 %
20 %
Molar Ellipticity (x10³ degree cm² dmol⁻¹)
80
60
40
20
0
-20
-40
190
200
210
220
230
240
250
Wavelength (nm)
B
rmsd (Å) MATKHGKNSWKTLYLKISFLGCKVVVLLKR
All atom 9.9 8.4 6.4 6.3 4.5 2.4 2.7 1.2 0.8 0.5 0.9 0.6 0.5 0.8 0.5 0.9 0.6 0.7 0.9 0.9 0.3 0.7 0.9 0.7 0.7 0.7 0.8 1.1 2.1 4.1
Backbone 9.4 7.9 6.0 4.4 3.1 2.4 1.1 0.7 0.4 0.3 0.3 0.3 0.2 0.2 0.2 0.2 0.3 0.4 0.4 0.5 0.3 0.4 0.3 0.3 0.4 0.3 0.4 0.6 1.8 3.3
C
~37 Å
~15 Å

Figure 4

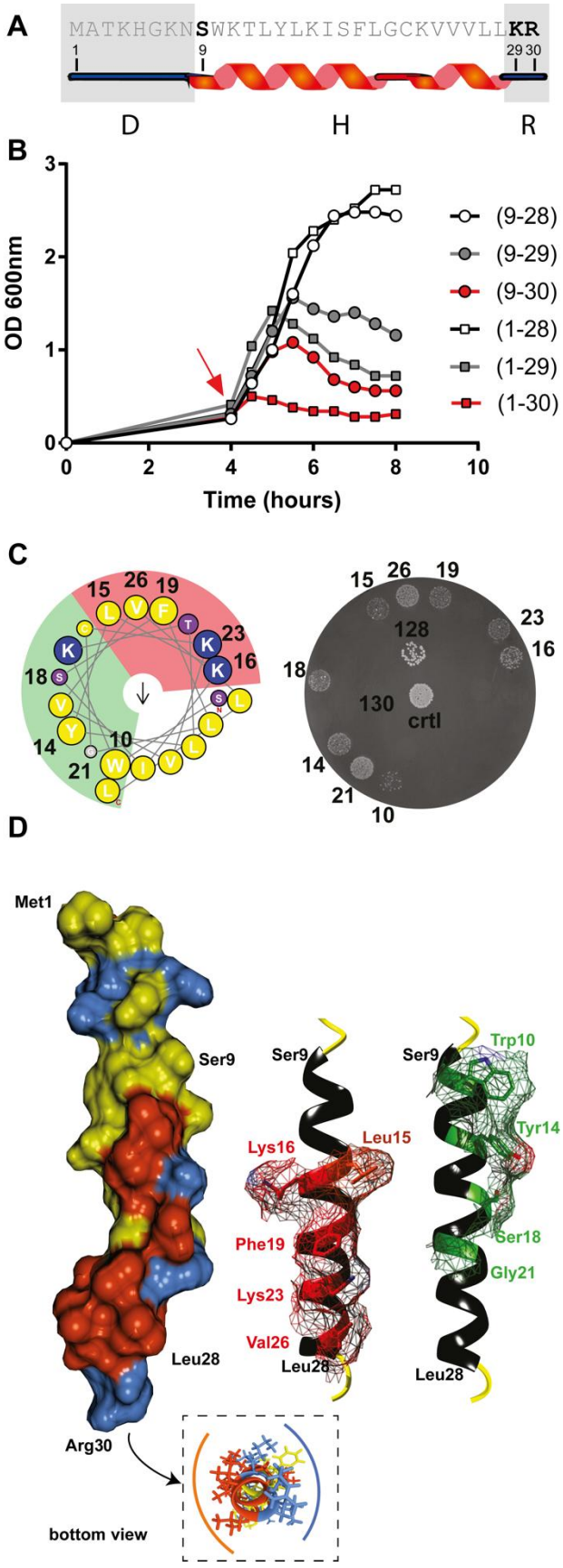
A
MATKHGKNSWKTLYLKISFLGCKVVVLLKR
1
9
29 30
D
H
R
B
OD 600nm
Time (hours)
(9-28)
(9-29)
(9-30)
(1-28)
(1-29)
(1-30)
C
15 26 19
23 16
18
14 10
21
128
130
crtl
D
Met1
Ser9
Leu28
Arg30
bottom view
Ser9
Lys16
Leu15
Phe19
Lys23
Val26
Leu28
Ser9
Trp10
Tyr14
Ser18
Gly21
Leu28

Graphical abstract